AlGaN-based MQWs grown on a thick relaxed AlGaN buffer on AlN templates emitting at 285 nm

Xiaogai Li, S Sundaram, Pierre Disseix, G Le Gac, S Bouchoule, G Patriarche, F Réveret, Joël Leymarie, Y El Gmili, T Moudakir, et al.

AlGaN-based MQWs grown on a thick relaxed AlGaN buffer on AlN templates emitting at 285 nm

X. Li,[1,2] S. Sundaram,[2] P. Disseix,[3] G. Le Gac,[3] S. Bouchoule,[4] G. Patriarche,[4] F. Réveret,[3] J. Leymarie,[3] Y. El Gmili,[2] T. Moudakir,[2] F. Genty,[5] J-P. Salvestrini,[2,6] R. D. Dupuis,[7] P. L. Voss,[1,2] and A. Ougazzaden[1,2,*]

[1]*School of Electrical and Computer Engineering, Georgia Institute of Technology, GT-Lorraine, 57070 Metz, France*
[2]*UMI 2958, Georgia Tech - CNRS, 57070 Metz, France*
[3]*Institut Pascal UMR 6602 CNRS, Université Blaise Pascal, 63171 Aubière, France*
[4]*LPN CNRS, UPR20, 91460 Marcoussis, France*
[5]*Supelec, LMOPS, EA4423, 57070 Metz, France*
[6]*Université de Lorraine, LMOPS, EA 4423, 57070 Metz, France*
[7]*Center for Compound Semiconductors and School of Electrical and Computer Engineering, Georgia Institute of Technology, Atlanta, Georgia 30332, USA*
[*]*aougazza@georgiatech-metz.fr*

Abstract: We report on the growth of $Al_{0.57}Ga_{0.43}N/Al_{0.38}Ga_{0.63}N$ MQWs grown on a relaxed $Al_{0.58}Ga_{0.42}N$ buffer on AlN template by Metal Organic Vapor Phase Epitaxy. The MQW structure is designed so that the strain in the quantum wells induced by their lattice mismatch with barriers is sufficient to enhance TE polarized emission (E-field ⊥ c). A 630-nm thick relaxed $Al_{0.58}Ga_{0.42}N$ buffer grown on AlN template serves as a pseudo-substrate to release the strain in the barriers and to avoid related defects or composition fluctuation in the active region. Thin (< 2 nm) quantum wells allow preservation of the overlapping of electron and hole wavefunctions considering the strong quantum-confined Stark effect in AlGaN-based MQW structures. Scanning transmission electron microscopy (STEM) coupled to energy-dispersive X-ray spectroscopy (EDX) analysis is used to optimize the growth conditions and to determine the composition of wells and barriers. Optical characterizations of the grown structure reveal a well-defined band-edge emission peak at 285 nm. Based on macro-transmission measurements and simulations, the absorption coefficient of the wells is estimated to be 3×10^5 cm^{-1} (E-field ⊥ c), attesting that the oscillator strength is preserved for these AlGaN MQWs with high Al content, which is promising for efficient surface-emitting devices in the deep ultra-violet (DUV) region.

OCIS codes: (160.4670) Optical materials; (230.3670) Light-emitting diodes; (260.7190) Ultraviolet; (230.5590) Quantum-well, -wire and -dot devices.

References and links

1. A. Fujioka, K. Asada, H. Yamada, T. Ohtsuka, T. Ogawa, T. Kosugi, D. Kishikawa, and T. Mukai, "High-output-power 255/280/310 nm deep ultraviolet light-emitting diodes and their lifetime characteristics," Semicond. Sci. Technol. **29**(8), 084005 (2014).
2. V. N. Jmerik, E. V. Lutsenko, and S. V. Ivanov, "Plasma-assisted molecular beam epitaxy of AlGaN heterostructures for deep-ultraviolet optically pumped lasers," Phys. Status Solidi A **210**(3), 439–450 (2013).
3. Z. Lochner, X.-H. Li, T.-T. Kao, M. M. Satter, H. J. Kim, S.-C. Shen, P. D. Yoder, J.-H. Ryou, R. D. Dupuis, K. Sun, Y. Wei, T. Li, A. Fischer, and F. A. Ponce, "Stimulated emission at 257 nm from optically-pumped AlGaN/AlN heterostructure on AlN substrate," Phys. Status Solidi A **210**(9), 1768–1770 (2013).
4. S. Gautier, T. Aggerstam, A. Pinos, S. Marcinkevičius, K. Liu, M. Shur, S. M. O'Malley, A. A. Sirenko, Z. Djebbour, A. Migan-Dubois, T. Moudakir, and A. Ougazzaden, "AlGaN/AlN multiple quantum wells grown by MOVPE on AlN templates using nitrogen as a carrier gas," J. Cryst. Growth **310**(23), 4927–4931 (2008).
5. H. R. Alaei and H. Eshghi, "Theoretical modeling for quantum-confined Stark effect due to internal piezoelectric fields in GaInN strained quantum wells," Phys. Lett. A **374**(1), 66–69 (2009).

#225937 - $15.00 USD Received 30 Oct 2014; revised 22 Dec 2014; accepted 23 Dec 2014; published 21 Jan 2015

6. H.-Y. Ryu, I.-G. Choi, H.-S. Choi, and J.-I. Shim, "Investigation of light extraction efficiency in AlGaN deep-ultraviolet light-emitting diodes," Appl. Phys. Express **6**(6), 062101 (2013).
7. T. Kolbe, A. Knauer, C. Chua, Z. Yang, S. Einfeldt, P. Vogt, N. M. Johnson, M. Weyers, and M. Kneissl, "Optical polarization characteristics of ultraviolet (In)(Al)GaN multiple quantum well light emitting diodes," Appl. Phys. Lett. **97**(17), 171105 (2010).
8. K. B. Nam, J. Li, M. L. Nakarmi, J. Y. Lin, and H. X. Jiang, "Unique optical properties of AlGaN alloys and related ultraviolet emitters," Appl. Phys. Lett. **84**(25), 5264–5266 (2004).
9. M. Leroux, F. Semond, F. Natali, D. Byrne, F. Cadoret, B. Damilano, A. Dussaigne, N. Grandjean, A. Le Louarn, S. Vézian, and J. Massies, "About some optical properties of AlxGa1−xN /GaN quantum wells grown by molecular beam epitaxy," Superlattices Microstruct. **36**(4-6), 659–674 (2004).
10. M. Leroux, S. Dalmasso, F. Natali, S. Helin, C. Touzi, S. Laügt, M. Passerel, F. Omnes, F. Semond, J. Massies, and P. Gibart, "Optical characterization of $Al_xGa_{1-x}N$ alloys (x<0.7) grown on sapphire or silicon," Phys. Status Solidi B **234**(3), 887–891 (2002).
11. S. L. Chuang and C. S. Chang, "K·P Method for strained wurtzite semiconductors," Phys. Rev. B **54**(4), 2491–2504 (1996).
12. J. E. Northrup, C. L. Chua, Z. Yang, T. Wunderer, M. Kneissl, N. M. Johnson, and T. Kolbe, "Effect of strain and barrier composition on the polarization of light emission from AlGaN/AlN quantum wells," Appl. Phys. Lett. **100**(2), 021101 (2012).
13. S. V. Ivanov, D. V. Nechaev, A. A. Sitnikova, V. V. Ratnikov, M. A. Yagovkina, N. V. Rzheutskii, E. V. Lutsenko, and V. N. Jmerik, "Plasma-assisted molecular beam epitaxy of Al(Ga)N layers and quantum well structures for optically pumped mid-UV lasers on c-Al_2O_3," Semicond. Sci. Technol. **29**(8), 084008 (2014).
14. H. Murotani, Y. Yamada, H. Miyake, and K. Hiramatsu, "Silicon concentration dependence of optical polarization in AlGaN epitaxial layers," Appl. Phys. Lett. **98**(2), 021910 (2011).
15. J. Baur, K. Maier, M. Kunzer, U. Kaufmann, and J. Schneider, "Determination of the GaN/AlN band offset via the (-/0) acceptor level of iron," Appl. Phys. Lett. **65**(17), 2211–2213 (1994).
16. M. B. Nardelli, K. Rapcewicz, and J. Bernholc, "Strain effects on the interface properties of nitride semiconductors," Phys. Rev. B **55**(12), R7323–R7326 (1997).
17. N. Binggeli, P. Ferrara, and A. Baldereschi, "Band-offset trends in nitride heterojunctions," Phys. Rev. B **63**(24), 245306 (2001).
18. F. Bernardini and V. Fiorentini, "Macroscopic polarization and band offsets at nitride heterojunctions," Phys. Rev. B **57**(16), R9427–R9430 (1998).
19. G. Martin, A. Botchkarev, A. Rockett, and H. Morkoç, "Valence-band discontinuities of wurtzite GaN, AlN, and InN heterojunctions measured by x-ray photoemission spectroscopy," Appl. Phys. Lett. **68**(18), 2541–2543 (1996).
20. G. Rakotonanahary, "Spectroscopie des transitions excitoniques dans des puits quantiques GaN/AlGaN," thèse de doctorat (PhD) en Physique de l'université Blaise-Pascal-Clermont-Ferrand II, 159 p (2011).
21. J. J. Hopfield, "Fine structure in the optical absorption edge of anisotropic crystals," J. Phys. Chem. Solids **15**(1-2), 97–107 (1960).
22. S. Gautier, C. Sartel, S. Ould-Saad, J. Martin, A. Sirenko, and A. Ougazzaden, "GaN materials growth by MOVPE in a new-design reactor using DMHy and NH_3," J. Cryst. Growth **298**, 428–432 (2007).
23. H. J. Kim, S. Choi, D. Yoo, J.-H. Ryou, R. D. Dupuis, R. F. Dalmau, P. Lu, and Z. Sitar, "Modulated precursor flow epitaxial growth of AlN layers on native AlN substrates by metal-organic chemical vapor deposition," Appl. Phys. Lett. **93**(2), 022103 (2008).
24. M. E. Hawkridge, Z. Liliental-Weber, H. J. Kim, S. Choi, D. Yoo, J.-H. Ryou, and R. D. Dupuis, "Erratic dislocations within funnel defects in AlN templates for AlGaN epitaxial layer growth," Appl. Phys. Lett. **94**(17), 171912 (2009).
25. M. A. Moram and M. E. Vickers, "X-ray diffraction of III-nitrides," Rep. Prog. Phys. **72**(3), 036502 (2009).
26. Y. L. Tsai, C. L. Wang, P. H. Lin, W. T. Liao, and J. R. Gong, "Observation of compositional pulling phenomenon in $Al_xGa_{1-x}N$ (0.4<x<1.0) films grown on (0001) sapphire substrates," Appl. Phys. Lett. **82**(1), 31–33 (2003).
27. H. Y. Lin, Y. F. Chen, T. Y. Lin, C. F. Shih, K. S. Liu, and N. C. Chen, "Direct evidence of compositional pulling effect in $Al_xGa_{1-x}N$ epilayers," J. Cryst. Growth **290**(1), 225–228 (2006).
28. B. Liu, R. Zhang, J. G. Zheng, X. L. Ji, D. Y. Fu, Z. L. Xie, D. J. Chen, P. Chen, R. L. Jiang, and Y. D. Zheng, "Composition pulling effect and strain relief mechanism in AlGaN/AlN distributed Bragg reflectors," Appl. Phys. Lett. **98**(26), 261916 (2011).
29. Z. Chen, Y. Pei, S. Newman, D. Brown, R. Chung, S. Keller, S. P. DenBaars, S. Nakamura, and U. K. Mishra, "Growth of AlGaN/GaN/AlGaN double heterojunction field-effect transistors and the observation of a compositional pulling effect," Appl. Phys. Lett. **94**(17), 171117 (2009).
30. G. B. Stringfellow, "Compositional ordering in semiconductor alloys," Proc. MRS **312**, 35–46 (1993).
31. J. Tersoff, "Stress-driven alloy decomposition during step-flow growth," Phys. Rev. Lett. **77**(10), 2017–2020 (1996).
32. P. Venezuela, J. Tersoff, J. A. Floro, E. Chason, D. M. Follstaedt, F. Liu, and M. G. Lagally, "Self-organized growth of alloy superlattices," Lett. to Nat. **397**(6721), 678–681 (1999).
33. B. Reuters, M. Finken, A. Wille, B. Holländer, M. Heuken, H. Kalisch, and A. Vescan, "Relaxation and critical strain for maximum In incorporation in AlInGaN on GaN grown by metal organic vapour phase epitaxy," J. Appl. Phys. **112**(9), 093524 (2012).

#225937 - $15.00 USD Received 30 Oct 2014; revised 22 Dec 2014; accepted 23 Dec 2014; published 21 Jan 2015

34. P. Bogusławski, K. Rapcewicz, and J. J. Bernholc, "Surface segregation and interface stability of AlN/GaN, GaN/InN, and AlN/InN {0001} epitaxial systems," Phys. Rev. B **61**(16), 820–826 (2000).
35. B. N. Pantha, R. Dahal, M. L. Nakarmi, N. Nepal, J. Li, J. Y. Lin, H. X. Jiang, Q. S. Paduano, and D. Weyburne, "Correlation between optoelectronic and structural properties and epilayer thickness of AlN," Appl. Phys. Lett. **90**(24), 241101 (2007).
36. K. Pantzas, G. Patriarche, D. Troadec, S. Gautier, T. Moudakir, S. Suresh, L. Largeau, O. Mauguin, P. L. Voss, and A. Ougazzaden, "Nanometer-scale, quantitative composition mappings of InGaN layers from a combination of scanning transmission electron microscopy and energy dispersive x-ray spectroscopy," Nanotechnology **23**(45), 455707 (2012).

1. Introduction

There is a strong demand for semiconductor light sources emitting in the DUV region for a wide variety of potential applications such as sterilization, water/air purification, optical imaging systems, spectroscopy, or high density storage systems. III-nitrides are potential candidates because of their interesting properties including tunable band gap covering the entire UV spectral range, thermal and chemical stability. However, compared with InGaN-based visible laser diodes or LEDs, the development of DUV light sources based on AlGaN material system is still a challenge. First, Al-rich AlGaN epilayers suffer from cracks or high dislocation density due to their large lattice mismatch with conventional sapphire or SiC substrates. AlGaN superlattices have been used in the literature as strain-relieving buffer between thick AlN layers and MQWs [1–3]. However this requires restrictive condition for complex layer-by-layer growth, moreover the active region still remains under high strain (the strain $|\varepsilon|$ in the barriers > 0.9%). Besides, AlGaN MQWs suffer from the strong quantum-confined Stark effect (QCSE) induced by piezoelectric and spontaneous polarization, which leads to the separation of electrons and holes and reduces significantly the emission efficiency [4,5]. In addition, c-plane AlGaN alloys also exhibit anisotropic optical polarization properties: E-field $\perp$ c polarized emission (which will be referred to as TE polarization) decreases when compared to the emission polarized along the c axis (E-field // c) as the Al composition increases for the deep UV wavelength, which is detrimental to surface-emission. This is attributed to the arrangement of the valence bands at the Γ point of Brillouin zone [6–10], leading to the lower TE efficiency of AlGaN-based DUV lasers or LEDs.

This paper reports on the design and fabrication of a MQW structure: $Al_{0.57}Ga_{0.43}N/Al_{0.38}Ga_{0.62}N$ MQWs grown on a relaxed $Al_{0.58}Ga_{0.42}N$ buffer using AlN templates on sapphire as a substrate. The MQW structure is designed to maximize the oscillator strength of the optical transition for TE polarization. A relaxed AlGaN buffer is used to release the excess strain in the barriers. Structural and optical characterizations have been performed to optimize the growth conditions and to assess the optical quality of the DUV MQW structures.

2. Design of the structure

In AlGaN alloys, the order of the two upper valence bands is modified with respect to binary GaN. Apart from the modification of the electric band structure, alloying also leads to a modification of the optical polarization properties of the interband transitions which influences the performance of the devices. In GaN, the upper valence band corresponds to the heavy hold band of Γ_9 symmetry, while the second one corresponds to the light hole band of symmetry Γ_7. For an aluminum composition typically higher than 10%, the energy order of these two bands reverses and the band of Γ_7 symmetry becomes the upper valence band [8,9]. This energy crossover between AlN and GaN is also accompanied by a switching of the valence band state symmetry. The topmost Γ_7 valence band is governed by p_z-like state. The following bands (Γ_9 and lower Γ_7) are governed by p_x and p_y-like states. So, if the three valence bands are labeled according to their zone center wavefunctions, the appropriate notation for AlN but also for AlGaN with high Al composition becomes CH (crystal field split-off band), HH (heavy hole band) and LH (light hole band) from top to bottom. The oscillator strength of the optical transitions is then modified and consequently the interband absorption coefficients (and stimulated-emission coefficients) are changed. In particular, the

#225937 - $15.00 USD Received 30 Oct 2014; revised 22 Dec 2014; accepted 23 Dec 2014; published 21 Jan 2015

oscillator strength between the conduction band and the upper Γ_{7CH} valence band, which becomes the fundamental transition, is highly reduced with increasing Al fraction for the configuration where the electric field is perpendicular to the c axis [8,9].

However, it is possible to restore the amplitude of the oscillator strength by imposing some strain in the AlGaN QW, which can affect the valence band states and the selection rules [11–14]. The strain is due to the lattice mismatch between barriers and wells which have different Al content. Thus, the barrier composition can be chosen to provide sufficient compressive strain in the wells, and to enhance the TE-polarized optical transition. The band structure and the optical interband matrix elements of AlGaN compounds were carried out by using **k.p** formalism for strained wurtzite semiconductors taking into account both valence band mixing due to crystal field and spin orbit effects and strain effect [11]. For the design of the AlGaN/AlGaN MQW structure, envelop function simulations taking into account strain and built-in electric fields have been performed. Considering the large scatter of valence-band offset (VBO) values reported in the literature (0.3 eV to 0.7 eV for GaN/AlN) [15–19], we use the experimental value of 0.5 eV determined by Baur *et al.* [15] for the VBO of GaN/AlN interface in the absence of strain. This value has been already tested on GaN/AlGaN QWs with a good agreement between calculations and experimental data [20]. The band diagram for the AlGaN/AlGaN heterostructure is then constructed by distributing the bandgap bowing on the conduction and valence bands of each alloy and by adding the strain effects induced by the lattice mismatch between the two materials [9,11,20,21]. The relative oscillator strength modeling is calculated by evaluating the matrix element between conduction and valence bands.

The strong electric-field in AlGaN quantum wells due to both piezoelectric and spontaneous polarization is around 1.15 $MV \cdot cm^{-1}$ and tends to separate the electrons and holes. To solve this problem, ultra-thin wells below 2 nm must be considered so that the oscillator strength obtained is not counteracted by the QCSE.

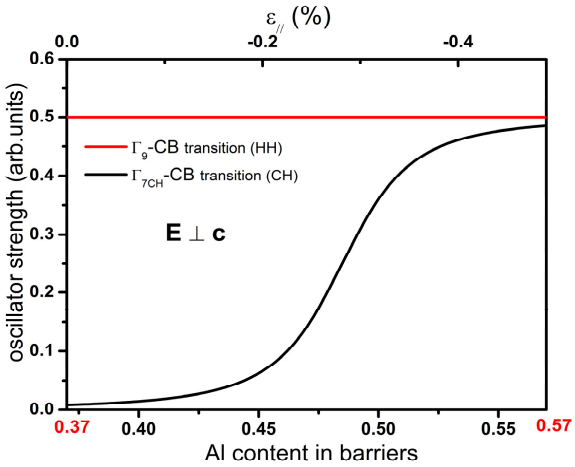

Fig. 1. Relative oscillator strengths for the optical transitions between the valence bands (Γ_7 (CH) and Γ_9 (HH)) and conduction band (CB) in an AlGaN/AlGaN quantum well as a function of the Al composition in the barriers, with Al content in the well fixed to x_{Al} = 0.37. The corresponding strain in the well is also reported in the top axis. Calculations consider that the barriers are strain-free and QWs are fully-strained on AlGaN barriers.

To achieve emission at a wavelength of around 280 nm, the Al composition of the well was chosen to be x_{Al} = 0.37 and the well thickness was fixed to 1.7 nm in the calculations. The thickness of barriers was fixed to 10 nm. The calculated values of the relative oscillator strengths for E perpendicular to c axis (TE polarization) are displayed in Fig. 1 as a function of the Al composition in the barriers. The uppermost valence bands of würtzite nitrides are formed out of *p* orbitals with wave functions combining $|X\rangle$, $|Y\rangle$ and $|Z\rangle$ symmetries. The

#225937 - $15.00 USD Received 30 Oct 2014; revised 22 Dec 2014; accepted 23 Dec 2014; published 21 Jan 2015

anisotropic strain mixes these valence band states and the polarization properties of the interband transitions are thus modified. When the biaxial stress increases with the increase of Al content in the barriers, the band-to-band oscillator strength of the fundamental transition involving Γ_7-valence band (crystal field split-off hole band (CH)) increases up to 0.5, which corresponds to the value of the oscillator strength of the transition involving the Γ_9-valence band (heavy hole). The CH valence band is no longer purely governed by p_z states but arises from a mixing between p_x, p_y and p_z states and is therefore not forbidden for TE polarization. The compressive strain increases the weight of p_x, p_y-like states at the expense of p_z-like states. So, the optimal Al content in barriers is designed to be 0.57 (± 0.01), for which the strain (−0.5%) introduced in the wells is sufficient to enhance TE-polarized optical transition and therefore surface emission. The above calculations assume no strain in the AlGaN barrier material. Practically, in order to release excess strain in the barriers, it is necessary to start the growth of the active region from a pseudo-substrate with barrier lattice mismatch as small as possible. AlN templates grown on c-Al_2O_3 wafers are appropriate substrates for the growth of Al-rich AlGaN MQW structures, however, AlN shows a lattice mismatch of 1% with $Al_{0.57}Ga_{0.43}N$ barriers. Hence, a thick, relaxed $Al_{0.57}Ga_{0.43}N$ layer has to be inserted before the MQW growth, acting as a latticed-matched buffer. Figure 2 presents the final design of the MQW structure.

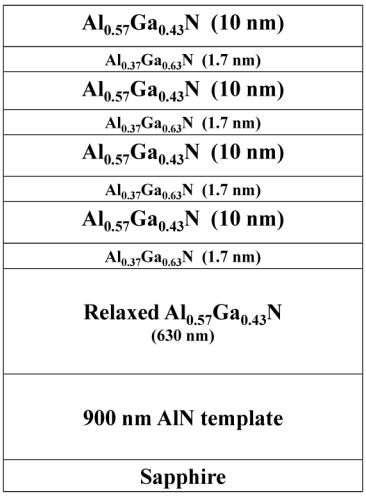

Fig. 2. Design of the AlGaN/AlGaN MQW structure grown on a relaxed AlGaN buffer on AlN template for emission wavelength at 280 nm.

3. Experimental details

The growth was performed in a MOVPE T-shape reactor [22] at 1000 þC under 100 Torr. Hydrogen was used as carrier gas. Trimethyl-aluminum (TMAl), thrimethyl-gallium (TMGa) and NH_3 were used as precursors for aluminum, gallium and nitrogen, respectively. 900-nm thick AlN templates on c-axis sapphire were used as substrates. Double-side polished c-Al_2O_3 wafers were used to allow for the optical transmission experiments. The AlN layer was grown by standard two-step heteroepitaxial growth and the dislocation density was considered to be high (> 10^9 cm^{-2}) as determined by XRD rocking curve [23,24]. For the growth of AlGaN layers, the TMAl/III ratio in the gas phase was varied in order to obtain different Al incorporation values, while the V/III ratio was kept constant. AlGaN layers of different thicknesses were also grown with a fixed TMAl/III ratio in order to investigate the composition fluctuation caused by strain-relaxation. The growth rate was determined from the in situ reflectance oscillations for thick layers, and by fitting the Pendellosung fringes of 2θ-ω scans for the thickness of thin layers. It was moreover confirmed by STEM analysis.

#225937 - $15.00 USD Received 30 Oct 2014; revised 22 Dec 2014; accepted 23 Dec 2014; published 21 Jan 2015

The growth of the MQW structure was performed following the design of Fig. 2. The barriers and the buffer layer were grown under the same conditions and 4 wells were inserted by regulating the TMGa flow rate. The structural characterization of the MQWs was carried out using high-resolution X-ray diffraction (XRD) measurements which were performed in a Panalytical X'pert Pro MRD system with Cu Kα radiation. The MQW structure was further investigated by high-angle annular dark field scanning transmission electron microscopy (HAADF-STEM) equipped with EDX for composition evaluation. The STEM lamellas were prepared using focused ion beam (FIB) etching. The optical properties were investigated by photoluminescence (PL) and depth-resolved cathodoluminescence (CL) techniques. The PL excitation at 266 nm was provided by the second harmonic generation of a continuous laser or or by a Q-Switched laser with a repetition rate of 20 kHz and 400ps pulse duration. The emission is analyzed by a 1 m focal length monochronometer and detected by a CCD camera. Both the optical excitation and light collection are from sample surface. Optical transmission measurements were performed under Xenon arc lamp excitation for determination of the absorption band-edge and absorption coefficients in the wells.

4. Results and discussion

4.1 Composition calibration with buffer relaxation

In order to obtain a good control over composition and relaxation for AlGaN buffer growth, the relationship between composition and TMAl/III ratio as wells as thickness and relaxation has been established. The strain state (plastic relaxation) has been determined by XRD asymmetric reciprocal space mappings (RSMs). It was verified for one AlGaN sample from RSM measurements along 6 asymmetric φ reflections of the würtzite lattice [25], that the tilt disorientation could be neglected in the following XRD spectra analysis. Then the composition has been determined based on the relaxation value and diffraction peak positions in symmetric 2θ-ω scans [25].

For the fully-strained thin layers below critical thickness, Al composition in the solid phase is plotted in Fig. 3 as function of TMAl/(TMAl + TMGa) ratio in the gas phase. The Al content varies linearly with the TMAl relative concentration, as commonly reported in the literature. Additionally, the AlGaN growth rate, shown in the inset, varies linearly with the total III elements flow (TMAl + TMGa) while the V/III ratio remains constant, which indicates that the growth occurs in a mass transport limited regime.

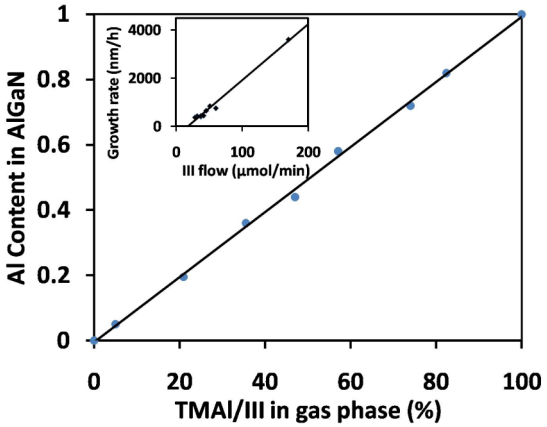

Fig. 3. Al composition of AlGaN layers fully-strained on AlN templates plotted as a function of TMAl/(TMAl + TMGa) ratio. The inset shows the growth rate versus total flow rate of (TMAl + TMGa).

However, when the thickness of the single AlGaN layer was increased under the same TMAl/III ratio so that the layer relaxed, it was observed that the average Al content in the layer decreased. Figure 4 shows the RSMs for the two samples grown under the same

#225937 - $15.00 USD Received 30 Oct 2014; revised 22 Dec 2014; accepted 23 Dec 2014; published 21 Jan 2015

TMAl/III of 57% but having different thicknesses: the 29-nm thick AlGaN is fully-strained on AlN template and shows an Al content of 0.57 (± 0.01), while for the 350-nm thick layer, showing a 55% relaxation, the Al content is only 0.47 (± 0.01).

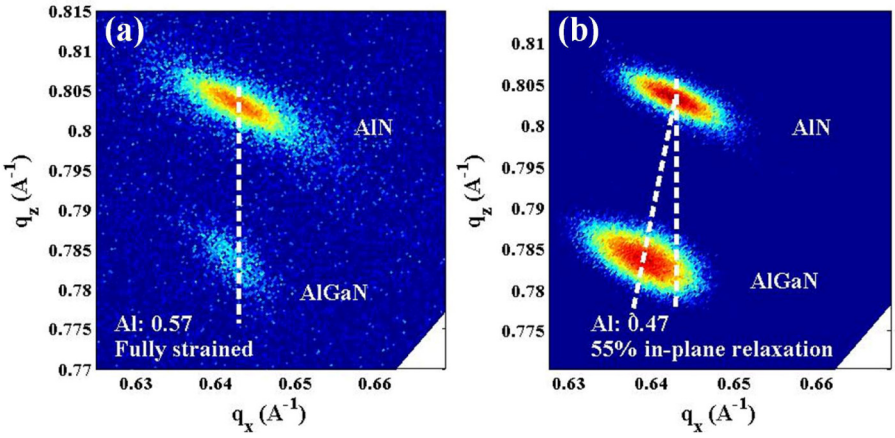

Fig. 4. (1 1 –2 4) Reciprocal Mapping for the (a): 29-nm thick AlGaN fully strained on AlN template and (b): 350-nm AlGaN layer with 55% relaxation on AlN template. Both samples are grown under a fixed TMAl/III ratio of 57%.

This composition fluctuation during AlGaN relaxation has generally been ascribed to the composition pulling effect [26–29]. G.B. Stringfellow *et al.* explained that the excess lattice mismatch energy would perturb the solid composition towards the composition which minimizes mismatch (composition pulling effect) [30]. The smaller adatoms will be incorporated preferentially at steps having relative compressive strain, and larger adatoms under relatively tensile strain [31,32]. But very few studies have considered AlGaN layers grown on AlN template which would be under compressive strain.

In the present investigation, as shown in Fig. 5, a decrease in the Al composition of AlGaN layers is evidenced when the layer thickness (and hence the layer relaxation) is increased. For three different TMAl/III ratios in the gas phase, a clear Al content drop can be observed, confirming the composition pulling effect. In our case, AlGaN is under compressive strain on AlN, so in the initial stage when the layer is fully strained, AlGaN has a tendency towards higher Al content in order to minimize mismatch, while for the relaxed layer case, we see a lower Al content. Since Ga-N has a smaller bond energy than Al-N, Ga incorporation would be more controlled by the strain state than Al incorporation [33,34], which means that Ga atoms are expelled out for the initial stage under high compressive strain, and Ga incorporation increases when the layer is relaxed with lateral lattice increasing.

#225937 - $15.00 USD Received 30 Oct 2014; revised 22 Dec 2014; accepted 23 Dec 2014; published 21 Jan 2015

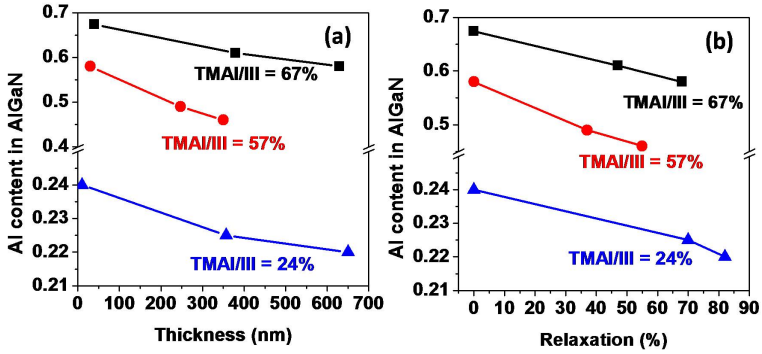

Fig. 5. Al content in the AlGaN single layers plotted as a function of (a) layer thickness, and (b) corresponding layer relaxation for three different TMAl/(TMAl + TMGa) ratios.

It should be noted that in our study, since a relaxed buffer is used, the barriers are almost lattice matched on this pseudo-substrate, which can also avoid composition fluctuation in the barriers caused by the pulling effect.

4.2 Growth and the characterization of the MQWs structure

Based on the design of the MQW structure and the study of the composition-relaxation relationship of AlGaN alloys mentioned above, the relaxed AlGaN buffer was grown on AlN template and its quality was verified before the growth of the quantum wells.

According to the growth rate measured by in situ reflectance, the layer thickness is of 630 nm, which was confirmed by STEM inspection. The layer shows a 70% plastic relaxation (the RSM is the same as the one in the inset in Fig. 7), and the Al composition estimated by fitting the (0 0 0 2) 2θ-ω scan shown in Fig. 6(a) is around 0.58 (± 0.01).

The (0 0 0 2) ω-scan of the AlN template and of the AlGaN buffer layer are shown in the inset of Fig. 6(a), respectively. In order to estimate screw and edge threading dislocation density, a series of skew symmetric ω scans of AlN template, 630 nm relaxed $Al_{0.58}Ga_{0.42}N$ buffer layer and 29 nm fully-strained $Al_{0.57}Ga_{0.43}N$ layer have been performed, which are demonstrated in Fig. 6(b). The tilt angle and twist angle can be separated, as expressed in Eq. (1), which is particularly useful for high defective layers such as AlN [25,35]:

$$\beta^2 = (\beta_{twist}^2 - \beta_{tilt}^2)\sin^2\chi + \beta_{tilt}^2 \tag{1}$$

where, β is FWHM angle and χ is inclination angle between the reciprocal lattice vector and the (0 0 0 1) surface normal.

Then the screw threading dislocation and edge threading dislocation density may be estimated by Eq. (2) [25,35]:

$$\begin{aligned} N_{screw} &= \beta_{tilt}^2 / (4.35 \times b_c^2) \\ N_{edge} &= \beta_{twist}^2 / (4.35 \times b_a^2) \end{aligned} \tag{2}$$

where, β_{tilt} and β_{twist} are the tilt and twist spread, the Burger vector of c-type TD (b_c) is 0.4982 nm for AlN and 0.5067 nm for $Al_{0.58}Ga_{0.42}N$, and the Burger vector of a-type TD (b_a) is 0.3112 nm for AlN and 0.3144 nm for $Al_{0.58}Ga_{0.42}N$. The resulting calculated screw and edge dislocation densities are ~9×10^9 cm^{-2} and ~2.7×10^{11} cm^{-2} for AlN template, ~6.7×10^9 cm^{-2} and ~1.6×10^{11} cm^{-2} for the thin fully-strained AlGaN layer, and ~5.6×10^9 cm^{-2} and ~1.5×10^{11} cm^{-2} for the relaxed AlGaN layer (FWHM determination and linear fitting lead to an estimated error of 15%). It should be noted that an overestimate is likely by this method, since one mixed dislocation combines both screw and edge component. The results confirm that the thick relaxed AlGaN buffer layer, which is used to release the strain in the barriers, is

#225937 - $15.00 USD Received 30 Oct 2014; revised 22 Dec 2014; accepted 23 Dec 2014; published 21 Jan 2015

grown with a good structural quality, i.e. without generating extra threading dislocations that would propagate into MQWs. Some annihilation of dislocations originating from the AlN template may even happen during the growth of the thick buffer layer, which could explain the reduced FWHM of the rocking curves.

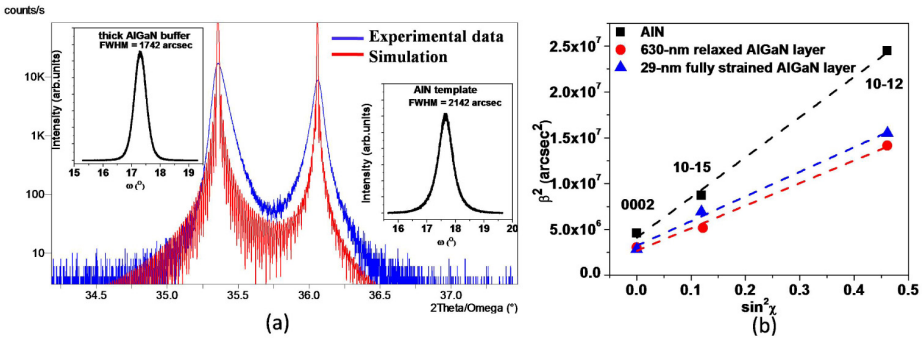

Fig. 6. (a) (0 0 0 2) 2θ-ω scan of the 630-nm relaxed $Al_{0.58}Ga_{0.42}N$ layer. Inset shows (0 0 0 2) rocking curves of AlN template and AlGaN layer; (b) skew symmetric scans to separate tilt angle and twist angle.

Four quantum wells were then grown on the relaxed AlGaN buffer on AlN template. The sample exhibits 2D morphology, and the root-mean square (RMS) surface roughness is 0.45 nm for 1 × 1 μm scan. Figure 7 shows the corresponding 2θ-ω scan of the sample. The diffraction pattern is dominated by the strong peaks related to the AlN template and the AlGaN relaxed buffer. Satellite diffraction peaks (SL) associated with the quantum wells can also be observed indicating abrupt interfaces between wells and barriers. The RSM in the inset shows the AlN template spot as well as the broader AlGaN buffer spot (and barriers). The signal from the thin quantum wells is too weak to be observed in RSM. From the symmetric 2θ-ω scan and asymmetric RSM, the composition and relaxation degree of the buffer were estimated: the average Al composition of buffer is ~0.58 (± 0.01) and the buffer has 70% relaxation, which is consistent with the results obtained for the buffer layer control sample (Fig. 6(a)). The composition and thickness of the wells could not be estimated accurately by just fitting 2θ-ω scan considering that the simulation of multi-layered structure is influenced by thickness and composition for each layer simultaneously. Further characterization using STEM and EDX is necessary in order to obtain more information about the quantum wells.

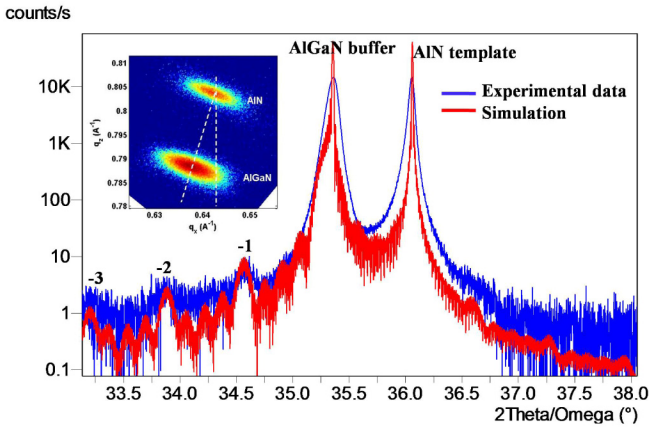

Fig. 7. (0 0 0 2) 2θ-ω scan for 4 quantum wells grown on a relaxed buffer on AlN template and the simulation of the structure which used values obtained by XRD, STEM and EDX analysis. The RSM of (1 1 −2 4) reflection is shown in the inset.

#225937 - $15.00 USD Received 30 Oct 2014; revised 22 Dec 2014; accepted 23 Dec 2014; published 21 Jan 2015

Figures 8(a) and 8(b) show the HAADF-STEM image of the quantum wells and of the upper part of the AlGaN buffer layer. The barriers thickness is measured to be 10 ~11 nm from intensity profiles and the wells thickness is of 1.6 ~1.8 nm. It can be observed that after each well there is an Al-rich layer which is presumably caused by a switch between precursors that can be optimized for the planned future work.

The average composition of barriers could be determined from EDX quantitative analysis and was found to be 0.57 (± 0.015). The k-factors used for the EDX quantification have been calibrated using thick AlN and GaN layers layers epitaxially grown on a silicon substrate. All calibration samples were prepared by FIB (the thickness of the slices is comprised between 60 to 80 nm). The systematic control of the stoichiometry (ratio between the III elements and the nitrogen content measured) ensures to be the right conditions for quantitative analysis (with accurate k-factors). The accuracy of the EDX analysis is estimated to be 1% (except with nitrogen where the precision is rather ± 2%). The results of the quantitative analysis (composition in atomic %) does not vary by more than ± 1% when the slice thickness varies in the range from 60 nm to 80 nm.

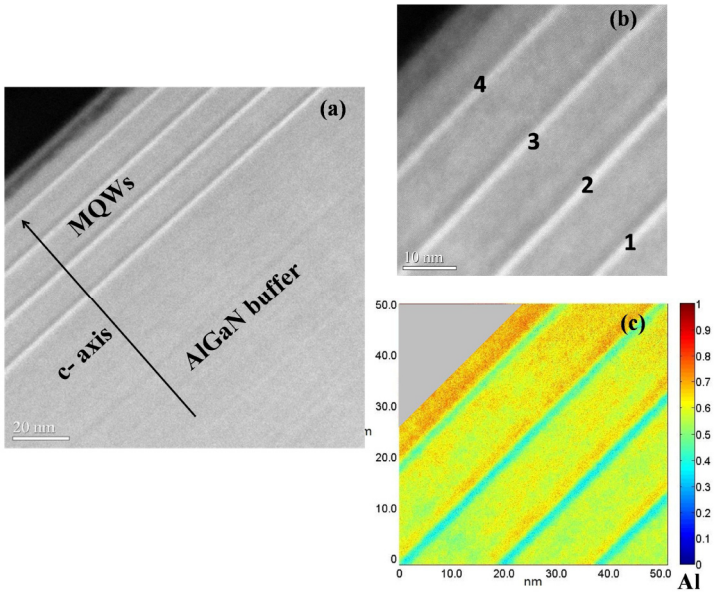

Fig. 8. (a) Cross-section High-angle Annular Dark Field Scanning Transmission Electron Microscopy (HAADF-STEM) images taken along the <1 1 –2 0> zone axis for MQWs and buffer layer; (b) High magnification of HAADF-STEM images; (c) Al composition map obtained from (b).

Since the spatial resolution of the EDX analysis is typically of 2 nm, high-resolution HAADF-STEM images have been used to estimate the composition of the thin quantum wells following a procedure proposed in [36]. The electron beam scattered intensity for each point M of the background-subtracted HAADF STEM image can be expressed as:

$$I(M) = d(M) \times K \times \sum_i x_i Z_i^{\alpha} \qquad (3)$$

where d (M) is the STEM slice thickness at point M, K is a proportionality factor depending on the number of atoms per unit volume in the lattice, the label i corresponds to atom i, x_i is the relative proportion of atom i (at point M), Z_i is its atomic number, and the value of power α is typically close to 2.

For the $Al_xGa_{1-x}N$ layers ($x = x_{Al}$), Eq. (3) can be rewritten as:

#225937 - $15.00 USD Received 30 Oct 2014; revised 22 Dec 2014; accepted 23 Dec 2014; published 21 Jan 2015

$$\frac{I_x(M)}{d_x(M)} = \frac{K}{2} \times Z_{Ga}{}^{\alpha} [a(\alpha) - b(\alpha) \times x] \quad (4)$$

where $a(\alpha) = 1 + \frac{Z_N{}^{\alpha}}{Z_{Ga}{}^{\alpha}}$, and $b(\alpha) = 1 - \frac{Z_{Al}{}^{\alpha}}{Z_{Ga}{}^{\alpha}}$

In order to use Eq. (4), the background-subtracted intensity I_x (M) is corrected from slight variations in the STEM slice thickness variations (d_x (M)) by comparing the intensity of the HAADF-STEM images at points where the EDX quantitative analysis predicts a nearly constant Al composition (in the AlGaN buffer, in the barriers). The thickness variation is extrapolated from these points for the whole HAADF image. A slight, regular and nearly linear variation of the thickness is observed, except at the very top surface of the epitaxial structure where a sharper variation of the slice thickness seems to occur. This region is therefore discarded from the analysis.

Then, the value of power α and of the proportionality constant K can be retrieved from points in the AlGaN buffer layer and in the AlN template, where x_{Al} is given by the EDX quantitative analysis. It is moreover assumed that K is constant for the range of materials considered. Given the values of $Z_{Ga} = 31$, $Z_{Al} = 13$, $Z_N = 7$, and α lying in the range of 1.6 to 2 [36], it is found that the best consistency with the experimental values in AlGaN buffer and AlN template are obtained for $\alpha = 2$ in our case.

The complete analysis results in a chemical mapping, as shown in Fig. 8(c). The average Al content in the barriers is accord with EDX value (x_{Al} ~0.57) and the average Al content in the wells is estimated to be x_{Al} ~0.38 (± 0.015). The thickness and composition values obtained from Figs. 8(a)-8(c) fit well the XRD experimental data shown in Fig. 7.

It is noticed that the composition of 4th well in the mapping is abnormally high (x_{Al} = ~0.50), and so as the last barrier (x_{Al} = ~0.67) which is not consistent with EDX value. It might be caused by the fact that the thickness variation near the top surface deviates from the linear extrapolation and hence leads to the inaccuracy of composition estimation from Z-contrast intensity.

4.3 Optical study of MQWs

Figure 9(a) displays cathodoluminescence (CL) spectra of the MQWs at 77K. Under a low excitation power of 3 keV corresponding to a penetration depth of the electron beam of typically 30 nm, a single emission peak from wells at 286 nm indicating that the carriers are mostly confined in the wells. When the excitation power is increased to 10 keV and the penetration depth of the excitation beam reaches 230 nm, a luminescence signal at 262 nm appears in addition to the emission of the wells, which is attributed to the barriers and buffer layer. The emission at 262 nm indeed corresponds to a bandgap energy of 4.73 eV, which is in agreement with the experimental composition of the barriers and buffer layer (x_{Al} ~0.57). At room temperature the increase of the barrier luminescence with respect to 77K is attributed to the thermal activation of carriers in the AlGaN layers (barriers or buffer layers). Due to the specific excitation induced by an electron beam, it is possible to observe the recombination of carriers localized in the AlGaN barriers or in the buffer layer. The energy of the electron beam allows probing the structure over various depths. In the case of an optical in-well pumping (excitation at 266 nm) as displayed in Fig. 9(b), the laser beam is mainly absorbed in the QWs and not in the barriers. Thus, only the luminescence of the wells is observed. However, it is found that both classical photoluminescence and cathodoluminescence provide the same QW emission line. The linewidth is 9.5 nm for PL at 77 K and 11.9 nm for PL at 300 K.

#225937 - $15.00 USD Received 30 Oct 2014; revised 22 Dec 2014; accepted 23 Dec 2014; published 21 Jan 2015

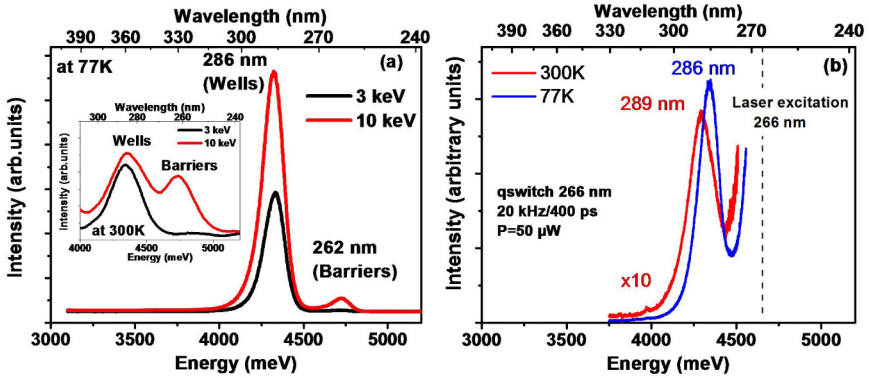

Fig. 9. (a) Cathodoluminescence (CL) spectra at 77 K (and at 300 K in the inset) for two different values of excitation power; (b) Photoluminescence (PL) at 77 K and 300 K under excitation of 266 nm.

Figure 10 shows the macro-transmission measurements (E-field ⊥ c configuration) at 77 K together with numerical simulations based on transfer matrix formalism. The experimental spectrum reveals the absorption edge of the barriers at 260 nm, while a 10% drop of transmission is observed at 281 nm due to absorption in the wells. It is worth noting that calculations fit the experimental results in a satisfying way. The absorption coefficients used in the simulation are also displayed in Fig. 10 for both barriers and wells. A weak absorption with linear energy dependence has been added in the barriers and the buffer in order to reproduce the overall decrease of the transmission signal. The latter might be caused by defects originated from the AlN template. The absorption coefficient in the wells is found to be as high as 3×10^5 cm^{-1}, which implies that the oscillator strength is preserved in the QWs despite the high aluminium composition.

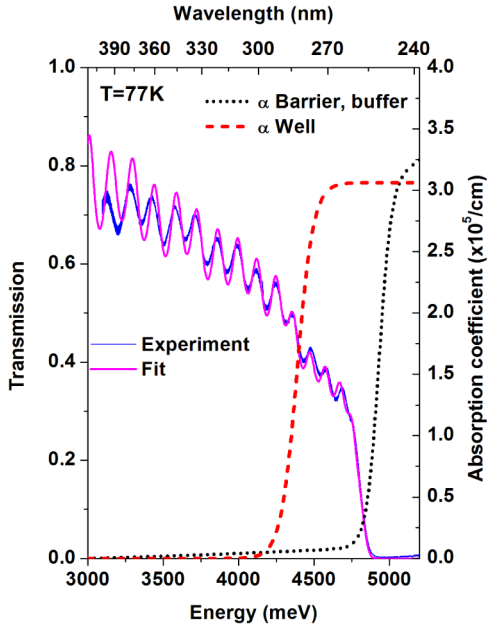

Fig. 10. Macro-transmission measurements and transfer-matrix simulation of MQWs together with absorption coefficients (α_{well}, $\alpha_{barrier,\ buffer}$) used in the simulation.

#225937 - $15.00 USD Received 30 Oct 2014; revised 22 Dec 2014; accepted 23 Dec 2014; published 21 Jan 2015

It is noted that the splitting between Γ_{7CH}-CB (fundamental) and Γ_9-CB transitions is evaluated to be equal to 32 meV. By considering the AlGaN broadening which is due to intrinsic alloy disorder and extrinsic inhomogeneities such as QW thickness fluctuations, it appears that the Γ_{7CH}-CB and Γ_9-CB transitions lie in the same energy range. The energy difference between these two transitions depends on several parameters (band offset, deformation potentials, effective masses…). So the absorption signal accounts for both transitions. However, it has been established through calculations displayed in section 2 that the strain preserves the oscillator strength of the fundamental transition (Γ_{7CH}-CB). Therefore it can be concluded that our MQW design with the use of relaxed buffer is promising for the fabrication of surface-emitting LED or lasers in DUV region.

5. Conclusion

In summary, an $Al_{0.57}Ga_{0.43}N$ / $Al_{0.38}Ga_{0.62}N$ MQW structure has been grown on a relaxed $Al_{0.58}Ga_{0.42}N$ buffer on AlN templates. The composition of the quantum wells was optimized so that the strain present in wells is sufficient to enhance TE-polarized (E-field $\perp$ c) emission. The relaxed AlGaN buffer on AlN template serves as pseudo-substrate, and in this way the barriers are almost strain-free which limits the formation of strain-related defects in the quantum wells. The structure exhibits an emission peak at 286 nm with a sharp linewidth at 77 K. Transmission measurements combined with simulations confirm a sufficient oscillator strength leading to an optical absorption coefficient in the wells as high as 3×10^5 cm^{-1}. The results represent an important step towards the development of DUV light sources, especially surface-emitting LEDs and lasers.

Acknowledgment

This work is supported by French ANR (Agence Nationale de la Recherche) in the framework of VESUVE project (ANR-11-BS03-0012). Dr. Konstantinos Pantzas of LPN is acknowledged for fruitful discussions and support for the chemical analysis of the HAADF-STEM images. Dr. David Troadec of IEMN (CNRS, Université Lille, RENATECH network) is acknowledged for the FIB etching. LPN-CNRS is a member of RENATECH national network of large micro-nanofabrication facilities. Dr. Jérémy Streque of UMI is acknowledged for his support on photoluminescence measurements. The authors thank two anonymous reviewers for their helpful comments and suggestions.